UCSF
UC San Francisco Previously Published Works

Title

Integration of the movement of signaling microclusters with cellular motility in immunological synapses

Permalink

Journal

ISSN

Authors

Beemiller, Peter
Jacobelli, Jordan
Krummel, Matthew F

Publication Date

DOI

Peer reviewed

Integration of Signaling Microcluster Movement with Cellular Motility in Immunological Synapses

Peter Beemiller[1], **Jordan Jacobelli**[1,2], and **Matthew F. Krummel**[1]

[1]Department of Pathology, University of California, San Francisco, San Francisco, CA, USA

Abstract

Immune synapses form between T cells and antigen presenting cells (APCs). Increasing evidence suggests synapses must form flexibly to accommodate ongoing motility and translation of the synapse. Time-lapse total internal reflection fluorescence (TIRF) microscopy revealed T cell receptor (TCR) signaling occurs during synapse translation. TCR microclusters in motile synapses did not flow directly into supramolecular activating complexes (SMACs) but were directed, independent of myosin II contractility, toward an F-actin poor "sink" region. Inward microcluster flow often followed collapse of the leading edge, suggesting that actin depolymerization regulated microcluster flow and formation of SMACs. Coordination of TCR movements with translocation of this sink reveals how T cells coordinate TCR signaling and microcluster flows in dynamic physiological synapses.

Introduction

T cells are activated when T cell receptors (TCRs) bind to agonist peptide bearing major histocompatibility complexes (pMHC) on antigen-presenting cells (APCs), triggering the collection of TCRs into micron scale signaling microclusters[1,2]. Studies of synapse formation revealed that microclusters flow inward radially, coalescing into a large, central supramolecular activating complex (cSMAC)[1,3,4]. Although cSMACs were initially suggested to be activating domains, it is now evident that signaling is predominantly supported by peripheral microclusters[5–7]. The formation of microclusters and SMACs depend on the actin cytoskeleton[6,8]. Synapse formation also requires adhesive interactions between other surface receptors, such as LFA1 on the T cell and ICAM on the APC[9]. These interactions are often enriched in a surrounding adhesive domain of the synapse, termed the peripheral SMAC (pSMAC)[2,4].

Initial antigenic stimulation is associated with ongoing T cell motility[10–12]. The resulting sequential interactions with APCs potentially allow T cells to sum stimuli from encounters[11,13]. These movements also suggest that immune synapses form against a continuously reorganizing cytoskeletal scaffold, and that TCRs are sorted into flexible domains. Given the fluid nature of T cell-APC contacts observed *in vivo*, it is unclear how well the uniformly organized, stationary synapses often seen *in vitro* represent physiological immune synapses.

Although some progress has been made analyzing TCR reorganizations in synapses *in situ*, technical constraints limit the spatiotemporal resolution there, preventing the analyses needed to understand TCR dynamics relative to the cytoskeleton during motility. How actin dynamics organize microcluster flows during motility and how SMACs are positioned in motile synapses are not understood. Total Internal Reflection Fluorescence (TIRF) microscopy of synapses formed on glass coverslip supported lipid bilayers are ideally suited to analyzing domain dynamics in motile synapses[2,14,15]. Much of this work, though, has been limited by the lack of model systems to analyze motility during signaling *in vitro*.

Using a lipid bilayer system for the activation of OT1^{+} T cells, we investigated microcluster dynamics in synapses formed during motility. We analyzed a range of stationary and motile synapses, allowing us to study the relationships between calcium signaling, microcluster dynamics, domain formation and motility. As observed *in vivo*[16,17], recognition of pMHC complexes reduced, but did not strictly halt, T cell motility. By analyzing microcluster, cSMAC and synapse movements, we show that microcluster flows in motile synapses aligned with cell movement, rather than moving toward existing cSMACs. Initiation of motility did not depend on cSMAC formation, but mature cSMACs moved in the direction of flowing TCRs and synapse translation. Using genetically deficient mice and pharmacologic inhibitor studies, we show that microcluster flow and generation of a central actin "sink" region did not require myosin II motors. Subsequent analysis of actin filament (F-actin) dynamics revealed a correlation between F-actin clearance and inward microcluster movement. Actin depolymerization was required to establish the F-actin poor interior sink region, toward which TCRs and cSMACs moved. These results demonstrate that actin depolymerization and central F-actin clearance organize TCR flow from the periphery and provide a model for immune synapse formation applicable to both stable and transient T-APC interactions.

Results

T cells Coordinate TCR Signaling with Motility

Previous studies have separately identified relationships between TCR-pMHC avidity and deceleration, as well as TCR-mediated calcium influx and motility arrest[17,18]. With limited exception, though[17,19], studies of T cell activation on bilayers have analyzed arrested T cells and have not addressed the interplay of pMHC density, calcium signaling and motility. To determine whether supported bilayers could recapitulate some of the activation dynamics seen *in vivo*[10,11], we investigated the relationship between agonist density, TCR signaling and T cell motility on a bilayer system. We developed a PEG-cushioned bilayer system for stimulating OT1^{+} T cells that presents ICAM and the SIINFEKL peptide bound to H-2K(b) MHC (see Supplementary Information). We generated bilayers with pMHCs densities ranging from the density measured on reference APCs (BMDCs pulsed with agonist peptide) down to five orders of magnitude lower; ICAM-1 was fixed at a density comparable to BMDCs (Supplementary Fig. 1).

Using these titrated bilayers, we analyzed how synapse motility and cytosolic calcium fluxes related to TCR ligand density. We measured cell displacement and intracellular calcium concentrations by time-lapse fura-2 ratiometric imaging[20] for each pMHC density. On bilayers that presented pMHC at densities comparable to reference BMDCs, OT1^{+} T cell blasts generated immediate and robust calcium influx (Fig. 1a, left). Cell motilities were greatly reduced relative to cells on non-stimulating bilayers (Fig. 1a, left-most vs. right-most graphs). However, moved at a relatively constant speed (1.9 μm/min). This effect was similar over three orders of magnitude of pMHC density (Supplementary Fig. 1). On bilayers loaded with 10,000-fold less pMHC (2.5×10^3 fg/ml), cells still underwent prominent rises in intracellular calcium, but overall cell speeds were twice as high (3.9 μm/

min, Fig. 1a). At the lowest pMHC density studied (loading with 2.5×10^2 fg/ml), T cells still generated calcium fluxes, but calcium concentrations peaked at roughly half that observed at high agonist doses. Cells crawling over these relatively low agonist densities moved at about half the speed of cells on non-stimulating bilayers (Fig. 1a, 3.8 μm/min vs 7.8 μm/min).

To quantify the relationship between cytosolic calcium and motility, we converted the fura-2 ratiometric intensities to calcium concentrations for the cells presented to bilayers loaded with 2.5×10^3 fg/ml pMHC. These cells were intermediately motile, but generated maximal calcium fluxes (Fig. 1a). We then graphed the instantaneous cell speed versus calcium concentration for these cells (Fig. 1b). Consistent with earlier work[18], cell speeds were generally inversely proportional to calcium concentration and calcium concentrations greater than ~0.75 μM resulted in arrest. However, cells with moderately elevated calcium concentrations moved at relatively high speeds, indicating that increased intracellular calcium concentration associated with TCR recognition did not necessarily block motility. Taken together, these results are in agreement with *in vivo* work demonstrating TCR-mediated 'deceleration', rather than 'arrest'[17].

Cell motility during bilayer engagement often followed two types of prototypical patterns. In 'paused' interactions, calcium concentrations rapidly spiked during a period of limited cell movement (Fig. 1c,d, top). In contrast, during 'motile' interactions, calcium concentrations intermittently increased as the cell continuously moved without pauses (Fig. 1c,d, bottom). Individual cells could display a range of motilities and calcium flux activities and transition between modes. This diversity led us to analyze how pMHC density affected the frequency of highly motile synapses and the relative amount of signaling generated during motility. As T cells on bilayers loaded with 2.5×10^3 fg/ml pMHC displayed large intracellular calcium increases and relatively high motility, we characterized synapses that moved at greater than the median speed of those cells (3.8 μm/min) as being highly motile. We observed a dose-dependent decrease in the number of high motility synapses ranging from 50% to 2% at the highest pMHC density (Fig. 1e). We then estimated the relative amounts of calcium signaling generated versus the cell displacements. The fura-2 ratiometric intensity timeseries for all cells were normalized by the total, above-baseline ratiometric intensity signal detected. On high agonist density bilayers, ~45% of the total elevated calcium signal that the cells generated occurred within 2 μm of binding sites (Fig. 1f, 2.5×10^7 fg/ml). On bilayers loaded with 2.5×10^3 fg/ml pMHC, the peak in intracellular calcium shifted slightly, to ~4 μm from binding sites. At the lowest pMHC density, intracellular calcium increases were not prominently localized to a particular distance from the binding site (Fig. 1f, 2.5×10^2 fg/ml). Together, this indicates that while T cell speeds were generally modulated by TCR signaling magnitude, T cells interacting with the stimulating bilayers coordinated TCR signaling with motility.

TCR Flow Couples with Cell Motility

Having observed that T cells could generate TCR signals in motile synapses, we examined whether TCR microcluster flows were also targeted to the cSMAC during motility, as predicted from stable synapses. To test this, we tracked CD3ζ-GFP microcluster movements using time-lapse TIRF microscopy of motile synapses formed by OT1^{+} T cell blasts expressing CD3ζ-GFP[1,21]. We analyzed periods of motility following a pre-motile phase encompassing cSMAC formation (Fig. 2a,b, and Supplementary Movie 1). We then compared TCR microcluster movements in arrested and motile synapses within individual cells.

Consistent with previous studies of stationary synapses[2,6], TCRs generally flowed inward along radial courses before motility started, resulting in a cSMAC (Fig. 2a, a prototypical example from a set of several hundred imaged synapses). However, the symmetric aspect of

the synapse was quickly lost, leading to a motile synapse (Fig. 2b and Supplementary Movie 1). Using intensity-based masks to define the synapse (the footprint of the T cell on the bilayer) and cSMAC regions, we calculated the paths followed by each (see Supplementary Information). The direction of movement changed three times to create four motility periods (Fig. 2b). The cSMAC path generally tracked the movement of the cell, including changes in direction (Fig. 2b, inset), but it was not positioned centrally and lagged behind the synapse centroid (Fig. 2c).

We then analyzed microcluster movements to determine if they were directed toward the cSMAC during motility. This revealed a pattern different from the premotility flows. Microcluster displacement vectors remained centripetally oriented. However, instead of flowing towards the cSMAC, microcluster vectors were shifted in the direction of motility and toward a region ahead of the cSMAC (Fig. 2d, insets and compare to Fig. 2a). This transition from cSMAC-oriented flow to motility-aligned flow was seen in all motile synapses in which microcluster flow could be analyzed.

To quantify aggregate microcluster flow, we calculated the median displacement vector for all the microclusters formed in each motility period. We found that the direction of this vector typically aligned with the direction of synapse movement during that period (Fig. 2e). The movement vector for the cSMAC also tracked the synapse movement vector, but often lagged relative to cell movement (Fig. 2e). Aggregate microcluster flow appeared to closely track synapse movement, even after changes in the direction of motility (Fig. 2f), while the cSMAC and cell movement vectors appeared loosely coupled and drifted apart over time (Fig. 2f, bottom). These data also suggested that microclusters and cSMACs moved toward a common, continuously moving target in motile synapses.

An F-actin Poor Region Is Central in Motile Synapse

We then analyzed whether synapse motility was dependent on cSMAC formation, and whether cSMACs were generally motile structures. We examined the motile synapses formed by CD3ζ-GFP–transduced OT1^{+} T cell blasts, analyzing the formation, positioning and movement of cSMACs relative to synapses. The cSMAC did not necessarily coalesce at the center of interfaces, even prior to motility, and cell displacement often appeared to begin before centralized TCR accumulations appeared (Fig. 3a and Supplementary Movie 2). In some synapses, cSMAC coalescence occurred as the cell transited the bilayer (Fig. 3b,c, motile cell), while in others, cSMACs aggregated prior to cell movement (Fig. 3b,c, paused cell). Alignment of image sequences by peak cSMAC areas and measurement of synapse speeds versus normalized cSMAC areas indicated no relationship between cSMAC aggregation and the onset of motility (Fig. 3d). The displacement of mature cSMACs was slightly lower than cell displacements, resulting in cSMACs positioning at the trailing edges of motile synapses (Fig. 3e).

To visualize cSMAC positioning relative to F-actin distributions in asymmetric and motile synapses, we fixed T cells following synapse formation, then permeabilized and stained the cells with Alexa Fluor 568-H57-597 anti-TCRβ and Alexa Fluor 488-phalloidin. In asymmetric synapses, cSMACs occupied an F-actin poor region near, but offset from, the center of synapses (Fig. 3f, left). In more polarized synapses characteristic of motility, cSMACs were positioned at the trailing edge of a cleared actin region (Fig. 3f, right), which occupied the interior of synapses. These results indicate that in mature cSMACs, the F-actin-poor interior is central to motile synapses and that cSMACs trail these domains.

Myosin II Is Dispensable for TCR Centralization and Synapse Motility

Having established that TCR microclusters and cSMACs moved toward an F-actin poor sink region, we wanted to identify cytoskeletal factors that orient these movements and form this domain. Although we previously reported successful cSMAC development following myosin II inhibition[22], myosin II was reported to be essential for signaling and microcluster movement into cSMACs in one study[23] or moderately important for TCR centralization rate in two others[24,25]. To determine whether myosin II regulated TCR centralization or general actin architecture in motile synapses, OT1^{+} T cell blasts were treated for 30 min with DMSO vehicle or 50 μM (−)-blebbistatin, an inhibitor of myosin II[26], then introduced to stimulating bilayers. Following synapse formation, cells were fixed and stained to image TCRs and F-actin distributions. In mature control synapses, F-actin was abundant in the periphery and TCRs accumulated in the F-actin–poor interior (Fig. 4a). In asymmetric synapses, suggesting polarization and motility, the F-actin–poor region and cSMAC were positioned at the posterior. In cells treated with blebbistatin, generation of the F-actin–poor region and cSMACs were not affected (Fig. 4a). Likewise, in asymmetric synapses, repositioning of the F-actin–poor region and cSMAC to the posterior were not blocked.

Next, we measured the effect of blebbistatin on synapse motility. Cells loaded with CellTracker Orange were imaged on stimulating bilayers using 555±14 nm illumination to avoid blebbistatin-mediated crosslinking with ~491 nm light[27,28] (Supplementary Movie 3). Blebbistatin reduced median synapse speed from 2.0 μm/sec to 1.6 μm/sec (Fig. 4b), consistent with a role for myosin II in regulating crawling speed[29]. However, blebbistatin did not delay the onset of motility, indicating that myosin II was not required to initiate synapse motility (Fig. 4c).

We then addressed whether myosin II regulated microcluster movements. To complement the drug approach, we used a conditional myosin II knockout system with OT1^{+} T cell blasts derived from myosin IIA 'floxed' mice[30]. Myosin II was depleted by retroviral transduction with Cre-GFP, resulting in genetic excision of myosin IIA, the only myosin II expressed in T cells[22]. Analysis of Cre-GFP–transduced cells indicated that myosin II was typically depleted to ~20–30% that observed in control cells (Supplementary Fig. 2). For controls, GFP-transfected OT1^{+} T cells subjected to the same transduction and sorting procedure were used. To image TCR microcluster dynamics in these cells, TCRs were stained with non-blocking Alexa Fluor 568-H57-597 antibodies prior to introduction to bilayers (Supplementary Fig. 2).

Tracking of TCR microclusters in control, conditional myosin II knockout (cKO) and blebbistatin-treated cells indicated that centralization of TCRs was not affected by genetic or chemical interference with myosin II (Fig. 4d and Supplementary Movie 4). To quantify inward flow, we calculated centralization values for the microclusters (see Supplementary Information). Median microcluster centralization, speed and track straightness were not significantly affected by blebbistatin or conditional myosin II knockout (Fig. 4e).

To test for a tensioning defect[24], we compared the spreading of control, blebbistatin-treated and cKO cells onto stimulating bilayers. Under all three conditions, cells rapidly spread microcluster-rich synapses. Over time, synapse areas contracted and cSMACs formed. Neither blebbistatin nor genetic ablation of myosin II blocked this spreading dynamic or cSMAC coalescence (Fig. 4f). The cKO cells, but not blebbistatin-treated cells, generated greater synapse areas than control cells. However, synapse expansion and contraction appeared to proceed normally in these cells (Fig. 4g). Importantly, synapse spreading dynamics were quantitatively similar, as the rate of expansion was not affected by either method of inhibiting myosin II (Fig. 4h).

To determine whether the increased synapse areas of the cKO cells might represent a specific defect in myosin II–mediated tensioning, we measured synapse sizes for control and cKO cells relative to the cell volumes (see Supplementary Information). In the cKO cells, we found a small, statistically insignificant increase in the mean synapse radius relative to the volumetric radius (Fig. 4i), consistent with results demonstrating that myosin II did not modulate synapse area during TCR signaling[29]. As control and blebbistatin-treated cells generated identical synapse areas (Fig. 4g), we attribute the increased synapse area of the cKO cells to the increased size of myosin II–depleted cells (Supplementary Fig. 2).

F-actin Is Cleared From the Center of Synapses

The accumulation of TCRs into F-actin–poor regions independent of myosin II activity led us to analyze F-actin dynamics in spreading synapses. To image actin dynamics in living cells, we used Lifeact-GFP, a genetically encoded probe that binds F-actin non-disruptively and reports the subcellular density of F-actin[31]. The rate of change in Lifeact-GFP intensity reports whether a region is undergoing net actin polymerization or depolymerization.

To image F-actin dynamics during synapse spreading, OT1^{+} T cell blasts retrovirally transduced with Lifeact-GFP and stained with Alexa Fluor 568-H57-597 were introduced to stimulating bilayers. During spreading, we observed a band of increased Lifeact-GFP intensity at the periphery, indicating a high F-actin density region (Fig. 5a). We then analyzed F-actin dynamics in the interior in comparison to the 2 μm 'edge' region that was located beyond this band (Fig. 5a,b, the region between the grey and dashed grey lines). This edge region corresponds to the distal SMAC (dSMAC) or lamellopodial region[25]. We graphed the Lifeact-GFP intensity and edge region position along a line through one side of the expanding synapse (Fig. 5c). As the edge expanded outward, the position of the high Lifeact-GFP intensity region moved outward, consistent with actin polymerization driven expansion of the edge (Fig. 5c,d). Behind the spreading F-actin dense band, F-actin abundance decreased in the first 30 s, suggesting depolymerization (Fig. 5a,c).

We then quantified actin density changes in 1 μm^2 regions surrounding microclusters, separating the microclusters into edge- and interior-formed groups (Fig. 5b). In the edge region, Lifeact-GFP intensity increased until the end of spreading, indicating actin polymerization occurred throughout spreading (Fig. 5e). In the interior, the Lifeact-GFP intensity derivative was negative during expansion, indicating active clearance of F-actin from the interior (Fig. 5e). This finding indicated that coordinated actin polymerization and depolymerization organized synapse domains, and suggested that regional depolymerization might establish a low-density sink that directs TCR flows.

TCR Centralization Correlates with Depolymerization

We next analyzed TCR microcluster movements with respect to synapse spreading and formation of the F-actin–poor sink region. We first examined microcluster movements relative to synapse dynamics in CD3ζ-GFP OT1^{+} T cell blasts. Microcluster formation began immediately, and, as spreading completed, localized retractions began reshaping the synapse into a polarized structure (Fig. 6a, light-blue arrow heads and Fig. 6b). In many cells, we observed that edge collapse correlated with localized loss of F-actin and inward microcluster movement (Supplementary Fig. 3).

During spreading, TCRs, particularly those located close to synapse edges, tended to move outward with the edges (Supplementary Movie 5). To quantify microcluster centralization kinetics, we calculated the radial movements for the microclusters relative to the synapse center (Supplementary Fig. 3 and Supplementary Information). The radial displacement value was defined so that movements toward the cSMAC are positive and movements away

from the cSMAC are negative. To analyze the relationship between edge and microcluster movements, edge displacements were calculated at the cell edge proximal to each of the 111 microcluster tracks (the distance to the edge along the line from the cSMAC centroid and through the microcluster). Radial displacements were outward directed during spreading and transitioned to inward movement as the synapse approached its peak area (Fig. 6c, compare to Fig. 6b). As expansion ended, microcluster and edge radial displacements began increasing (Fig. 6c,d). This result indicated that TCR microcluster flows were sensitive to the same conditions that regulated expansion and contraction of synapses.

Next, we compared microcluster movements in the edge and interior relative to the instantaneous changes in F-actin density in the 1 μm^2 regions around microclusters using Lifeact-GFP (see Supplementary Information). Edge microclusters initially moved inward rapidly (3.9 μm/min), and then more slowly (1.1 μm/min) as they reached the interior of the synapse (Fig. 6e). When we analyzed the changes in F-actin density around edge microclusters relative to microcluster movements, we observed a correlation: while outward microcluster displacement, which occurred primarily during spreading, accompanied increasing F-actin density, inward movement associated with movement into decreasing F-actin density (Fig. 6f, r = −0.36, also Supplementary Fig. 3 and Movie 6). This suggested that local polymerization in the dSMAC did not drive inward flow of local microclusters.

Interior microclusters underwent little radial displacement during spreading, and did not begin to centralize for about 30 s (Fig. 6g). In contrast to edge microcluster movement, interior microcluster flow did not correlate with actin density changes (Fig. 6h, r = −0.02). However, the centralization of interior microclusters began around the time that the F-actin poor sink region appeared, suggesting it was important for centralization.

TCR Centralization Requires Actin Depolymerization

To test whether the formation of the low F-actin density regions regulated TCR microcluster flows, we specifically blocked actin depolymerization in T cells interacting with stimulating bilayers. While a number of actin polymerization inhibitors are available, jasplakinolide specifically blocks depolymerization in living cells by binding to and stabilizing actin filaments[32]. However, the effects of jasplakinolide are complex: at low doses, filaments are stabilized, inhibiting depolymerization, while at high doses, jasplakinolide severely alters cytoskeletal architecture and blocks polymerization[33]. Therefore, we developed a jasplakinolide treatment that did not inhibit synapse spreading, an actin polymerization–dependent process[34]. OT1^{+} T cell blasts stained with Alexa Fluor 568-H57-597 and DiO (a membrane dye) were treated with different concentrations of jasplakinolide for 15 min on ice before addition to bilayers. Treated with up to 50 nM jasplakinolide, cells exhibited no defect in spreading relative to control cells (Fig. 7a). At 100 nM jasplakinolide, though, synapse areas were reduced by 40%, equivalent to synapses formed after direct inhibition of polymerization with cytochalasin D (Fig. 7a), indicating impaired actin polymerization.

Jasplakinolide also inhibited cSMAC coalescence in a dose-dependent manner (Fig. 7b). 100 nM jasplakinolide rendered T cells completely incapable of generating cSMACs. 50 nM jasplakinolide, which did not block polymerization, substantially reduced the efficiency of cSMAC formation to 30% of the efficiency of control cells (Fig. 7b). Inhibiting depolymerization and cSMAC formation did not block TCR signaling, though, as control cells and cells treated with 50 nM jasplakinolide generated virtually identical calcium fluxes (Fig. 7c). We then performed time-lapse TIRF microscopy of Lifeact-GFP and TCRs in vehicle– and 50 nM jasplakinolide–treated OT1^{+} T cell blasts. In control cells, F-actin–poor interior regions appeared as TCR microclusters began to centralize (Fig. 7 d,e). In motile synapses, cSMACs were positioned behind this F-actin–poor region (Supplementary Movie 7). Jasplakinolide–treated cells also spread actin–rich footprints onto bilayers and generated

TCR microclusters (Fig. 7f). However, the actin-poor sink region failed to form in the jasplakinolide-treated cells, and TCR microcluster centralization was severely reduced (Fig. 7f,g). Microcluster centralizations (Fig. 7h) and speeds (Fig. 7i) were significantly reduced by 50 nM jasplakinolide. In addition, microcluster track straightness in jasplakinolide-treated cells was significantly reduced (Fig. 7j), suggesting that microclusters formed in the presence of jasplakinolide experienced greater confinement. These results demonstrate that actin depolymerization directs microcluster flow into regions of low F-actin density.

Discussion

The coordinated flow of microclusters into a single central accumulation of TCRs would seem to imply that the cSMAC serves as the organizational center of immune synapses. However, this model has not been tested previously to describe how T cells organize TCR clusters during dynamic interactions[11,13]. We were able to examine TCR microcluster dynamics in a motile setting, capturing an important aspect of *in vivo* T cell activation that has been missing from *in vitro* studies. While bilayers present an unlimited, uniform activation surface, *in vivo*, T cells may establish and break contacts with multiple, irregularly-shaped DCs. Therefore, the importance of continued motility and myosin motor–mediated force generation during activation will be underestimated on bilayers.

During spreading, TCRs near synapse edges appeared to be pushed outward by polymerizing actin. This might reflect associations between TCRs and barbed-end associated factors that initiate actin polymerization. Alternatively, these patches might represent non-ligated, or even sub-plasmalemmal, collections of TCRs that move anomalously. Ultimately, outward moving microclusters centralized similar to interior microclusters, suggesting they were, or developed into, signaling microclusters. Inward flow from the periphery was biphasic: initial, rapid centralization was associated with collapse of the dense lamellipodial actin meshwork, while slower centralization followed as microclusters moved into the interior. The slower centralization was likely associated with actin retrograde flow[6,8]. As retrograde flow is dependent on continued actin depolymerization[35], localized depolymerization in the interior sink provides a mechanism to guide TCRs to recycling regions. Organizing these flows likely requires the spatially regulated activity of cofilin, coronin and other related actin depolymerizing proteins[36]. A previous study that blocked TCR capping using cofilin mimetic peptides supports this hypothesis[37]. We propose that depolymerization generates a low viscosity 'sink' for inward microcluster flow. Under this model, the motive force is still polymerization[6,8]. However, a depolymerization-dependent mechanism, in which flows are regulated by regional viscosity reduction, has appeal; it would explain how TCRs move inward discontinuously[7] at maximum rates that approach actin retrograde flow, whereas actin flows continuously[8]. The incorporation of microclusters into cSMACs, then, would be due to microclusters and cSMACs being squeezed into the same actin-poor region. Developing cSMACs also coupled to synapse movement. However, there was hysteresis in cSMAC movement, suggesting passive coupling.

We initially reported that myosin II was deactivated in response to TCR triggering, and that inhibition did not prevent TCR centralization or conjugate formation[22]. In contrast, another study reported that myosin II motor was required for the movement of TCRs into cSMACs, maintenance of adhesion to APCs and continued signaling[23]. Another report employing blebbistatin suggested that myosin II mediated tension contributed to microcluster flow only in a brief, early phase of TCR centralization[24]. Finally, in a recent study using blebbistatin in Jurkat cells, it was reported that the contraction of actinmyosin II arcs, in concert with actin depolymerization, directs TCR transport[25]. Disparities between these studies might reflect distinct motor requirements in mouse T cells versus human T cells versus Jurkat cells,

differences in depletion efficiency, or comparing hand-selected cells that have taken up siRNA to unselected cells. A significant issue also arises in some experiments from the activation of protein crosslinking by blebbistatin with short wavelength illumination[27,28]. The viability of myosin II depleted T cells falls precipitously as levels drop below what we report, suggesting depleted cells might be fundamentally compromised. While myosin II tensioning might enhance centralization under some conditions, our data shows that it is dispensable.

It remains to be determined whether motile synapses are fundamentally different from current models of immunological synapses. Our observations do not suggest a mechanistic distinction between stationary and motile synapses. A flexible framework for synapse formation, as presented here, can describe both the unstable synapses seen in vivo, as well as highly-organized sedentary synapses. This model does not require a coordinate relationship between the cSMAC and microcluster flows. Instead, the F-actin-poor sink organizes TCR flows. This explains how synapses can organize signaling without motility arrest or the aggregation of TCRs into a cSMAC[16].

Methods

Mice

CD8^{+} OT1^{+} TCR-transgenic mice, which recognize the SIINFEKL peptide of ovalbumin bound to H-2K(b)[38], were obtained from Taconic, and then bred in-house. The floxed-MyH9 mice, described previously[30], were crossed with OT1^{+} mice. Mice were housed and bred at UCSF according to Laboratory Animal Resource Center guidelines. Protocols were approved by the Institutional Animal Care and Use Committee of the University of California.

Cells

OT1[+] T cell blasts were prepared from the lymph nodes of OT1^{+} mice. Cells were retrovirally transduced with CD3ζ-GFP or Lifeact-GFP Phoenix cell supernatants as described previously[39]. Conditional myosin II-deficient OT1^{+} T cell blasts were generated by transducing proliferating OT1^{+} MyH9[flox/flox] T cells with a Cre-GFP retroviral supernatant[30]. Blasts were used 4–6 days after stimulation. On the day of imaging, live T cells were collected, stained as required for experiments, washed and then held on ice in complete RPMI without phenol red indicator until used for imaging. To label surface TCRs, 2×10^6 cells were stained for 30 min on ice with 1 μg Alexa Fluor 568-labeled H57-597 anti-TCRβ in 0.1 ml complete RPMI without indicator.

To inhibit actin depolymerization, stained, washed cells on ice were treated with 25–100 μM jasplakinolide. After 15 min, cells were transferred to a pre-warmed bilayer well containing jasplakinolide at the same concentration used to treat the cells. To inhibit actin polymerization, cells were incubated with 10 μM cytochalasin D for 30 min at 37 C. To inhibit myosin II activity, 50 μM (−)-blebbistatin was added to cells for 30 min at 22 C before addition to a well pre-loaded with blebbistatin. Blebbistatin was loaded as a 100 μM racemic mixture of (+, inactive) and (−, active) enantiomers. DMSO vehicle was used as a control for drug treatments.

Reagents

H57-597 anti-TCRβ was purchased from Bio-X-Cell and conjugated to Alexa Fluor 568 at the UCSF hybridoma facility. The dodecahistidine-tagged extracellular domain of ICAM1 (his-ICAM) was purified from the supernatant of High Five cells transfected using a baculovirus expression system. The protein was purified using nickel-affinity resin,

followed by MonoQ, then Superdex FPLC. His-ICAM was labeled with Alexa Fluor 488 using Alexa Fluor 488 succinimidyl ester. Biotinylated H-2K(b) loaded with SIINFEKL was purchased from Beckman Coulter, or obtained from the NIH Tetramer Facility, and used in monomeric form.

Lipid Bilayers

Phospholipid mixtures consisting of 96.5% POPC, 2% DGS-NTA (Ni), 1% Biotinyl-Cap-PE and 0.5% PEG5,000-PE were mixed in a round bottom flask and dried. The following day, liposomes were prepared from the rehydrated lipid cakes by extrusion through 100 nm pore-size filters using a LiposoFast extruder (Avestin).

To setup lipid bilayers, liposomes dilutions were applied to a rigourously cleaned LabTek II chambered coverglass (Nalge Nunc). Excess liposomes were rinsed away, and bilayers then blocked in 1% bovine serum albumin in PBS (PBS-BSA). Streptavidin was loaded in PBS-BSA, and then the excess streptavidin washed away. His-ICAM and biotinylated pMHC were added to bilayers at loading concentrations of $2.5 \times 10^2 – 2.5 \times 10^7$ fg/ml biotinylated pMHC and 62.5–500 ng/ml his-ICAM. After loading proteins, bilayers were rinsed, inhibitors added if needed, and pre-warmed before applying cells.

To generate standardized bilayers, we measured the concentrations of his-ICAM and biotinylated pMHC on bilayers relative to cultured BMDCs pulsed with 100 ng/ml SIINFEKL peptide. Lipid bilayers were setup on silica microspheres (Bangs Labs) by the same procedure used for coverslip supported bilayers. Microsphere bilayer standards and BMDCs were stained for ICAM (YN1/1.7.4) and SIINFEKL:H-2K(b) (25-D1.16), and analyzed by flow cytometry. Except where indicated, stimulating bilayers refers to a bilayer loaded with his-ICAM and pMHC under conditions that generate similar protein presentation as compared to peptide-pulsed BMDCs.

Microscopy

A Zeiss Axiovert 200-M equipped with Laser TIRF slider was used to perform all imaging (Zeiss). For TIRF microscopy, a 1.45 NA, 100x Plan-Fluar or a 1.46 NA, 100x PlanApo objective lens were used. A DG-4 (Sutter Instruments) was used to provide epifluorescent illumination for fura-2 ratiometric imaging and CellTracker Orange imaging. A 1.3 NA, 40x PlanFluar objective was used for imaging cell movements in widefield. In two-color TIRF imaging, a DV2, two-channel simultaneous imaging system (Photometrics) with a 560 nm long pass dichroic filter and 525/50 nm and 605/70 nm bandpass emission filters was used to split the camera field into two image channels for simultaneous GFP and Alexa Fluor 568 imaging. Images were collected by one of two cameras: an Evolve emCCD (Photometrics) or a Stanford Photonics XR-10MegaZ iCCD camera (Stanford Photonics). For TIRF image sequences acquired using the iCCD camera, QED InVivo (Media Cybernetics) software was used. For TIRF, FRAP and Fura ratiometric images acquired by the emCCD camera, Metamorph software was used (Universal Imaging).

To image $OT1^+$ T cells interacting with the bilayers, 10^5 cells in 0.1 ml of complete RPMI without Phenol Red indicator were added to the 0.5 ml PBS volume overlaying the bilayer. For Fura ratiometric image time-lapse sequences, acquisition was started as soon as the first cells tethered to the bilayer (typically within 1 minute of addition of cells). Fura-2 component images, consisting of 340/10 nm or 380/10 nm excitation with emission recorded at 520/20 nm, were collected with 33–66 msec exposures at 15 s intervals for 20 min. For TIRF image time-lapses, cells undergoing initial spreading onto bilayers were located, and TIRF images acquired at 1 or 2 s intervals using 33–100 ms exposure lengths for 3–5 min. Cells were imaged until all cells had bound to the bilayers (typically 10–15 min) or, when

imaging jasplakinolide or blebbistatin treated cells, for 5 min after delivering cells into wells.

Image Analysis

All image arithmetic operations, for example: filtering, background subtraction, masking, and division, were performed in MATLAB (The Mathworks). TCR microcluster identification was perfomed using the polynomial fitting with Gaussian weight method[40]. Assignment of identified microclusters to tracks was performed in Imaris (Andor) by transferring the microcluster data using the ImarisXT MATLAB interface. Further track analyses, such as categorization of tracks by their time of formation or calculation of movement vectors, was performed after transferring the assembled tracks to data structures in MATLAB. Cell tracking was performed in Imaris using Fura-2 ratiometric images calculated and masked in MATLAB. Conversion of fura-2 ratiometric intensities to calcium concentrations was performed as described previously[41]. Detailed descriptions of the image processing routines can be found at the Nature Protocol Exchange.

Statistical analyses were performed in Prism (GraphPad Software). The Mann-Whitney U test or Student's t test, where appropriate, were used to compare samples. For comparing multiple groups, 1-way ANOVA ($\alpha = 0.05$) was used with Dunnett's post-test. The tests applied, resulting p-values, and sample numbers are reported in figure legends.

Supplementary Material

Refer to Web version on PubMed Central for supplementary material.

Acknowledgments

References

1. Krummel MF, Sjaastad MD, Wülfing C, Davis MM. Differential Clustering of CD4 and CD3ζ During T Cell Recognition. Science. 2000; 289:1349–1352. [PubMed: 10958781]

2. Grakoui A, et al. The immunological synapse: a molecular machine controlling T cell activation. Science. 1999; 285:221–227. [PubMed: 10398592]

3. Wülfing C, Davis MM. A Receptor/Cytoskeletal Movement Triggered by Costimulation During T Cell Activation. Science. 1998; 282:2266–2269. [PubMed: 9856952]

4. Monks CRF, Freiberg BA, Kupfer H, Sciaky N, Kupfer A. Three-dimensional segregation of supramolecular activation clusters in T cells. Nature. 1998; 395:82–86. [PubMed: 9738502]

5. Yokosuka T, et al. Newly generated T cell receptor microclusters initiate and sustain T cell activation by recruitment of Zap70 and SLP-76. Nat Immunol. 2005; 6:1253–1262. [PubMed: 16273097]

6. Varma R, Campi G, Yokosuka T, Saito T, Dustin ML. T cell receptor-proximal signals are sustained in peripheral microclusters and terminated in the central supramolecular activation cluster. Immunity. 2006; 25:117–127. [PubMed: 16860761]

7. Mossman KD, Campi G, Groves JT, Dustin ML. Altered TCR signaling from geometrically repatterned immunological synapses. Science. 2005; 310:1191–1193. [PubMed: 16293763]

8. Kaizuka Y, Douglass AD, Varma R, Dustin ML, Vale RD. Mechanisms for segregating T cell receptor and adhesion molecules during immunological synapse formation in Jurkat T cells. Proc Natl Acad Sci USA. 2007; 104:20296–20301. [PubMed: 18077330]

9. Dustin ML, Springer TA. T-cell receptor cross-linking transiently stimulates adhesiveness through LFA-1. Nature. 1989; 341:619–24. [PubMed: 2477710]

10. Miller MJ, Safrina O, Parker I, Cahalan MD. Imaging the Single Cell Dynamics of CD4+ T Cell Activation by Dendritic Cells in Lymph Nodes. J Exp Med. 2004; 200:847–856. [PubMed: 15466619]

11. Mempel TR, Henrickson SE, von Andrian UH. T-cell priming by dendritic cells in lymph nodes occurs in three distinct phases. Nature. 2004; 427:154–159. [PubMed: 14712275]

12. Celli S, Garcia Z, Bousso P. CD4 T cells integrate signals delivered during successive DC encounters in vivo. J Exp Med. 2005; 202:1271–1278. [PubMed: 16275764]

13. Gunzer M, et al. Antigen Presentation in Extracellular Matrix: Interactions of T Cells with Dendritic Cells Are Dynamic, Short Lived, and Sequential. Immunity. 2000; 13:323–332. [PubMed: 11021530]

14. Campi G, Varma R, Dustin ML. Actin and agonist MHC-peptide complex-dependent T cell receptor microclusters as scaffolds for signaling. J Exp Med. 2005; 202:1031–1036. [PubMed: 16216891]

15. Lee KH, et al. The Immunological Synapse Balances T Cell Receptor Signaling and Degradation. Science. 2003; 302:1218–1222. [PubMed: 14512504]

16. Friedman RS, Beemiller P, Sorensen CM, Jacobelli J, Krummel MF. Real-time analysis of T cell receptors in naive cells in vitro and in vivo reveals flexibility in synapse and signaling dynamics. J Exp Med. 2010; 207:2733–2749. [PubMed: 21041455]

17. Skokos D, et al. Peptide-MHC potency governs dynamic interactions between T cells and dendritic cells in lymph nodes. Nat Immunol. 2007; 8:835–44. [PubMed: 17632517]

18. Negulescu PA, Krasieva TB, Khan A, Kerschbaum HH, Cahalan MD. Polarity of T Cell Shape, Motility, and Sensitivity to Antigen. Immunity. 1996; 4:421–430. [PubMed: 8630728]

19. Sims TN, et al. Opposing Effects of PKCθ and WASp on Symmetry Breaking and Relocation of the Immunological Synapse. Cell. 2007; 129:773–785. [PubMed: 17512410]

20. Weiss A, Imboden J, Shoback D, Stobo J. Role of T3 Surface Molecules in Human T-Cell Activation: T3-Dependent Activation Results in an Increase in Cytoplasmic Free Calcium. Proc Natl Acad Sci USA. 1984; 81:4169–4173. [PubMed: 6234599]

21. Ehrlich JS, Hansen MDH, Nelson WJ. Spatio-Temporal Regulation of Rac1 Localization and Lamellipodia Dynamics during Epithelial Cell-Cell Adhesion. Dev Cell. 2002; 3:259–270. [PubMed: 12194856]

22. Jacobelli J, Chmura SA, Buxton DB, Davis MM, Krummel MF. A single class II myosin modulates T cell motility and stopping, but not synapse formation. Nat Immunol. 2004; 5:531–538. [PubMed: 15064761]

23. Ilani T, Vasiliver-Shamis G, Vardhana S, Bretscher A, Dustin ML. T cell antigen receptor signaling and immunological synapse stability require myosin IIA. Nat Immunol. 2009; 10:531–539. [PubMed: 19349987]

24. Yu Y, Fay NC, Smoligovets AA, Wu HJ, Groves JT. Myosin IIA modulates T cell receptor transport and CasL phosphorylation during early immunological synapse formation. PloS one. 2012; 7:e30704. [PubMed: 22347397]

25. Yi J, Wu XS, Crites T, Hammer JA. Actin Retrograde Flow and Acto-Myosin II Arc Contraction Drive Receptor Cluster Dynamics at the Immunological Synapse in Jurkat T-Cells. Mol Biol Cell. 2012; 23:834–852. [PubMed: 22219382]

26. Straight AF, et al. Dissecting temporal and spatial control of cytokinesis with a myosin II Inhibitor. Science. 2003; 299:1743–7. [PubMed: 12637748]

27. Kolega J. Phototoxicity and photoinactivation of blebbistatin in UV and visible light. Biochem Biophys Res Commun. 2004; 320:1020–1025. [PubMed: 15240150]

28. Sakamoto T, Limouze J, Combs CA, Straight AF, Sellers JR. Blebbistatin, a myosin II inhibitor, is photoinactivated by blue light. Biochemistry. 2005; 44:584–8. [PubMed: 15641783]

29. Jacobelli J, Bennett FC, Pandurangi P, Tooley AJ, Krummel MF. Myosin-IIA and ICAM-1 Regulate the Interchange between Two Distinct Modes of T Cell Migration. J Immunol. 2009; 182:2041–2050. [PubMed: 19201857]

30. Jacobelli J, et al. Confinement-optimized three-dimensional T cell amoeboid motility is modulated via myosin IIA-regulated adhesions. Nat Immunol. 2010; 11:953–961. [PubMed: 20835229]

31. Riedl J, et al. Lifeact: a versatile marker to visualize F-actin. Nat Methods. 2008; 5:605–607. [PubMed: 18536722]

32. Bubb M, Senderowicz A, Sausville E, Duncan K, Korn E. Jasplakinolide, a cytotoxic natural product, induces actin polymerization and competitively inhibits the binding of phalloidin to F-actin. J Biol Chem. 1994; 269:14869–14871. [PubMed: 8195116]

33. Bubb M, Spector I, Beyer BB, Fosen KM. Effects of Jasplakinolide on the Kinetics of Actin Polymerization. An explanation for certain in vivo observations. J Biol Chem. 2000; 275:5163–5170. [PubMed: 10671562]

34. Bunnell SC, Kapoor V, Trible RP, Zhang W, Samelson LE. Dynamic Actin Polymerization Drives T Cell Receptor–Induced Spreading: A Role for the Signal Transduction Adaptor LAT. Immunity. 2001; 14:315–329. [PubMed: 11290340]

35. Vallotton P, Gupton SL, Waterman-Storer CM, Danuser G. Simultaneous mapping of filamentous actin flow and turnover in migrating cells by quantitative fluorescent speckle microscopy. Proc Natl Acad Sci USA. 2004; 101:9660–9665. [PubMed: 15210979]

36. Delorme V, et al. Cofilin activity downstream of Pak1 regulates cell protrusion efficiency by organizing lamellipodium and lamella actin networks. Dev Cell. 2007; 13:646–62. [PubMed: 17981134]

37. Eibert SM, et al. Cofilin peptide homologs interfere with immunological synapse formation and T cell activation. Proc Natl Acad Sci USA. 2004; 101:1957–62. [PubMed: 14762171]

38. Hogquist KA, et al. T cell receptor antagonist peptides induce positive selection. Cell. 1994; 76:17–27. [PubMed: 8287475]

39. Friedman RS, Jacobelli J, Krummel MF. Surface-bound chemokines capture and prime T cells for synapse formation. Nat Immunol. 2006; 7:1101–8. [PubMed: 16964261]

40. Rogers SS, Waigh TA, Zhao X, Lu JR. Precise particle tracking against a complicated background: polynomial fitting with Gaussian weight. Phys Biol. 2007; 4:220–7. [PubMed: 17928660]

41. Grynkiewicz G, Poenie M, Tsien R. A new generation of Ca2+ indicators with greatly improved fluorescence properties. J Biol Chem. 1985; 260:3440–3450. [PubMed: 3838314]
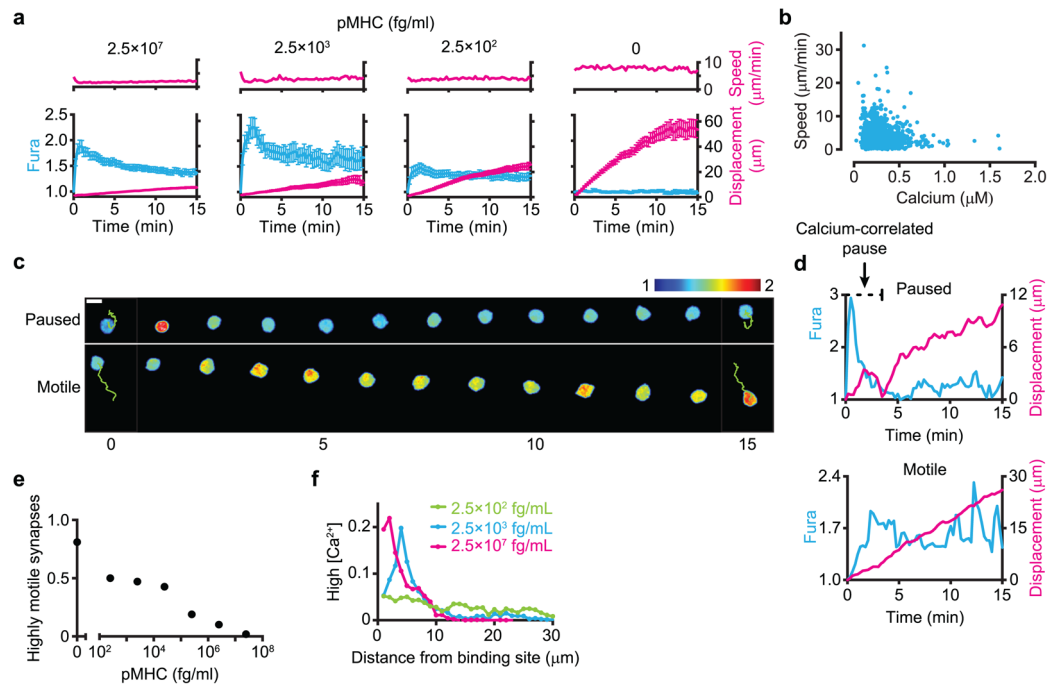
Figure 1. T cells remain motile during TCR signaling triggered by a large range of agonist doses
(**a**) Top: cell speeds; bottom: baseline-normalized fura-2 ratios (relative calcium concentrations) and displacements of cells interacting with bilayers loaded with the indicated concentrations of pMHC. Error bars represent the standard error of the mean (s.e.m.). Bilayers loaded with 2.5×10^7 fg/ml pMHC presented agonists at densities similar to peptide-pulsed BMDCs. (**b**) Speeds versus cytosolic calcium concentration of the cells interacting with bilayers loaded with 2.5×10^3 fg/ml pMHC. N = 96 cells. (**c**) Fura-2 ratiometric image sequences of prototypical synapses. Top: a paused synapse, where motility followed TCR signaling activity. Bottom: a motile synapse, where signaling occurred during motility. Images intensities were scaled to a normalized Fura-2 ratio intensity range of 1–2. For display purposes, images were filtered with a 0.4 µm σ Gaussian filter. Numbers below panels indicate time (min). Scale bar is 5 µm. (**d**) Fura-2 ratios and displacements for the cells in (**c**). (**e**) The fraction of cells that formed high motility synapses (3.8 µm/min average speed). Plot was generated using data from the cells sampled in (**a**) and from Supplementary Figure 1 (776 cells total). (**f**) The fraction of elevated calcium detected in the cells in (**a**) versus the cell displacement. Displacements were binned into 1 µm intervals relative to the site of bilayer binding. Plots in (**a**) represent >75 cells for each condition. Data were pooled from 2–4 bilayers per condition.
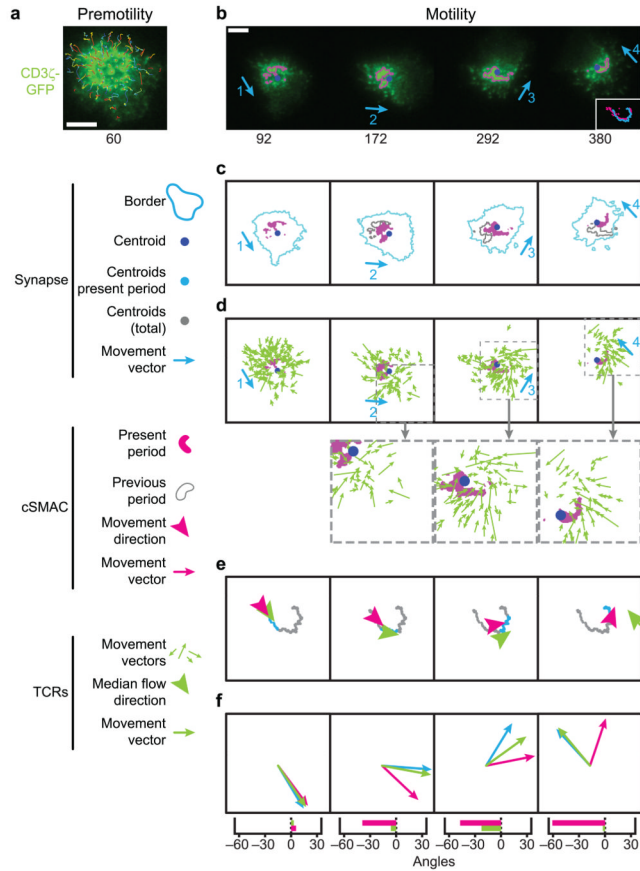
Figure 2. Microcluster flow aligns with movement in motile synapses

(**a, b**) Time-lapse TIRF images of a CD3ζ-GFP⁺ OT1⁺ T cell during synapse formation. Numbers below images indicate time (s) relative to the start of TCR centralization. Scale bars are 5 µm. (**a**) The microclusters paths prior to cell movement. (**b**) Synapse motility was divided into four periods based on the direction of movement (blue arrows). The borders of the cSMAC are shown in magenta. The paths followed by the cSMAC and synapse centroids are inset at lower right. (**c**) The cSMAC (magenta), synapse border (light-blue) and cSMAC border at the end of the preceding motility period (gray). (**d**) Displacement vectors for microclusters formed during each motility period overlaid onto the cSMAC mask at the start of the period (magenta). Dashed gray boxes show a magnified view of the indicated regions. (**e**) The median microcluster flow direction (green), and the direction of cSMAC movement (magenta) for each period. Arrowhead points are placed at the mean microcluster endpoint or cSMAC position at the end of the period. Cell centroids over the entire time series are shown (gray), with the centroids corresponding each period in blue. (**f**) Top: cell (blue), cSMAC (magenta) and median microcluster movement vectors (green) in each period, drawn with a common origin and scaled to the same magnitude. Bottom: angles between median microcluster movement vector and cell movement (green) and between cSMAC movement and cell movement (magenta) in each motility period. Data are representative of six synapses that transitioned to motility.
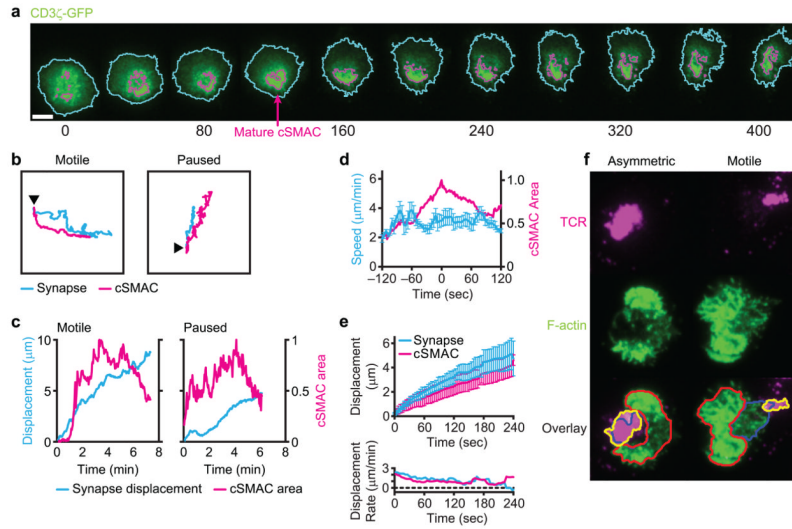
Figure 3. Synapse motility is independent of cSMAC formation
(**a**) Time-lapse TIRF microscopy images of CD3ζ-GFP during formation of a motile synapse. The synapse and cSMAC boundaries are outlined in light-blue and magenta, respectively. Scale bar is 5 μm. (**b**) The synapse (blue) and cSMAC centroids (magenta) over time for a motile and paused synapse. The cSMAC centroids were shifted to a common origin with the synapse, indicated by black arrow heads. (**c**) Synapse displacements and cSMAC areas (normalized to the maximum area) over time for the motile and paused synapses in (**b**). (**d**) Average speed of cells in motile synapses and the average normalized cSMAC area over time. The speed was smoothed with a 10-second moving window average. (**e**) Top: displacements over time of synapse and cSMAC centroids following cSMAC maturation (set to zero in the graph). Bottom: displacement rates for synapses and cSMACs. Error bars in (**d,e**) represent the standard deviation (s.d.). Nine synapses from a single set of bilayers were analyzed. (**f**) The cSMAC position and F-actin patterns in an asymmetric synapse (left) and motile synapse (right). The contours indicate: the border of the high F-actin density region (red), the border of the F-actin poor region (blue), and the cSMAC (yellow). 29 synapses were imaged and characterized as symmetric (not shown), asymmetric or motile. Approximately 30% of synapses were asymmetric and approximately 40% appeared motile.
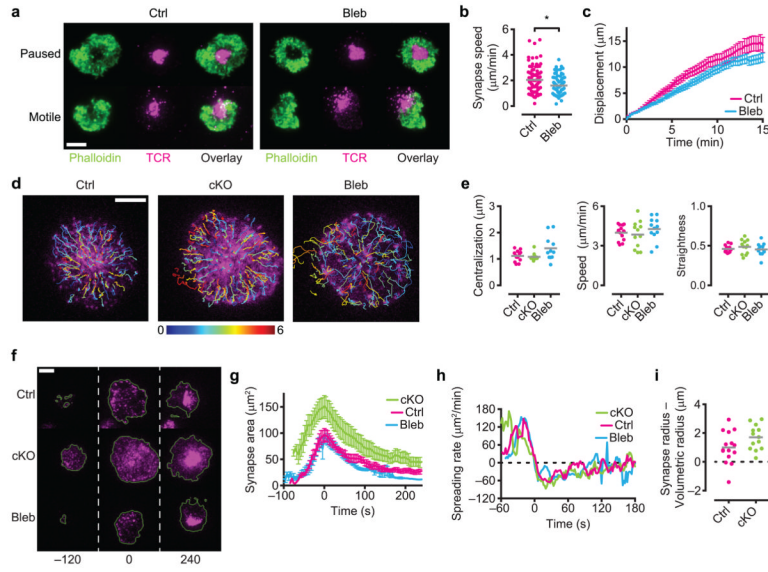
**Figure 4. TCR centralization and synapse dynamics are myosin II independent**
(**a**) F-actin staining and cSMAC positioning in paused and motile synapses formed by control and blebbistatin treated cells. Approximately 50 control and 50 blebbistatin treated cells on two bilayers were imaged. (**b**) Mean speeds of control and blebbistatin treated cell synapses (p = 0.003; Mann-Whitney). (**c**) Displacements of control and blebbistatin treated cells on stimulating bilayers. Data in (**b,c**) represent 76 control and 76 treated cells. Gray bars in (**c**) represent the median. (**d**) Microcluster paths overlaid onto TIRF images of Alexa Fluor 568-H57-597 stained TCRs in control, conditional myosin II knockout (cKO), and blebbistatin treated OT1^{+} T cells. Scale bars in (**a,d,f**) are 5 μm. (**e**) Median centralization, average microcluster track speeds and mean track straightness for microclusters in 16 control, 12 cKO and 12 blebbistatin treated cells. Gray bars represent the median centralization or mean speed/straightness of the groups. One-way ANOVA analysis of the track parameters did not reveal significant (p < 0.05) differences. (**f**) The spreading dynamics of a control, cKO, and blebbistatin treated cell. Numbers below images indicate time (s) relative to maximum synapse area. (**g**) Quantified synapse areas of control, cKO and blebbistatin treated cells. N = 7 for each condition. Error bars in (**c,g**) represent the s.e.m. (**h**) The temporal derivative of the synapse areas. Rates were smoothed using a 10-sec moving average filter. (**i**) Synapse radii relative to volumetric radii for 15 control and 14 cKO cells. Gray bars represent the median (p = 0.116; Mann-Whitney test).
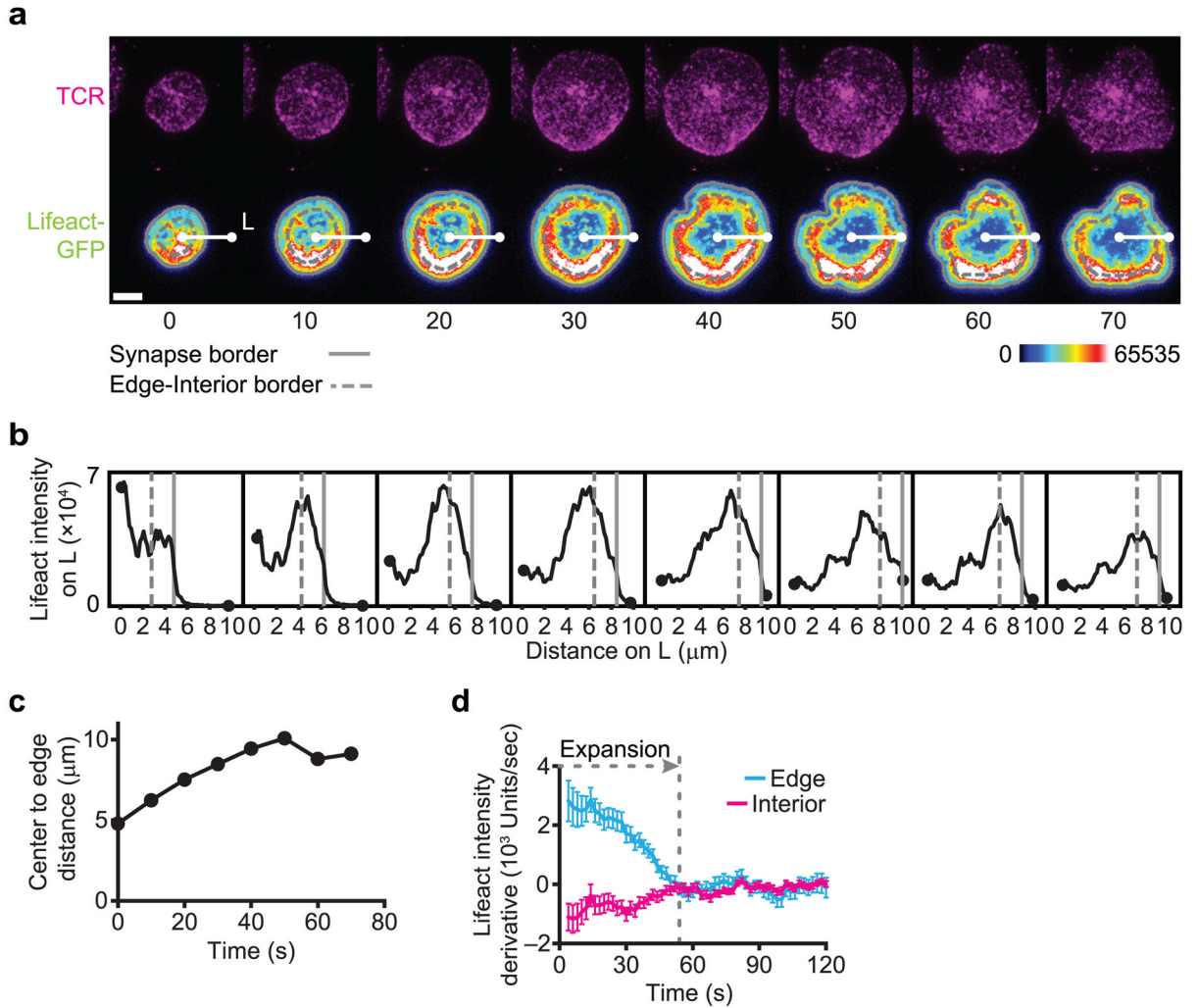
Figure 5. Actin polymerization and depolymerization organize synapses
(**a**) Time-lapse TIRF microscopy images of a Lifeact-GFP[+] OT1^{+} T cell blast spreading onto a stimulating bilayer. Top: Alexa Fluor 568-H57-597 labeled TCRs; bottom: Lifeact-GFP (pseudocolor look-up table shown at lower-right). Numbers below image are time (s). Scale bar is 5 μm. (**b**) Linescan intensities for the 10 μm line L in (**a**). Intensities are the average of 3 pixels (0.48 μm). The solid gray line in (**a**) and (**b**) indicates the synapse border; the dashed gray line is 2 μm from the cell edge. (**c**) Distance to the cell edge along the line L. (**d**) The changes in Lifeact-GFP intensites over time (change in intensity units per second) in the 1 μm^2 regions around the interior and edge microclusters. The dashed vertical line indicates the end of the spreading period. Data are representative of 8 synapse spreading.
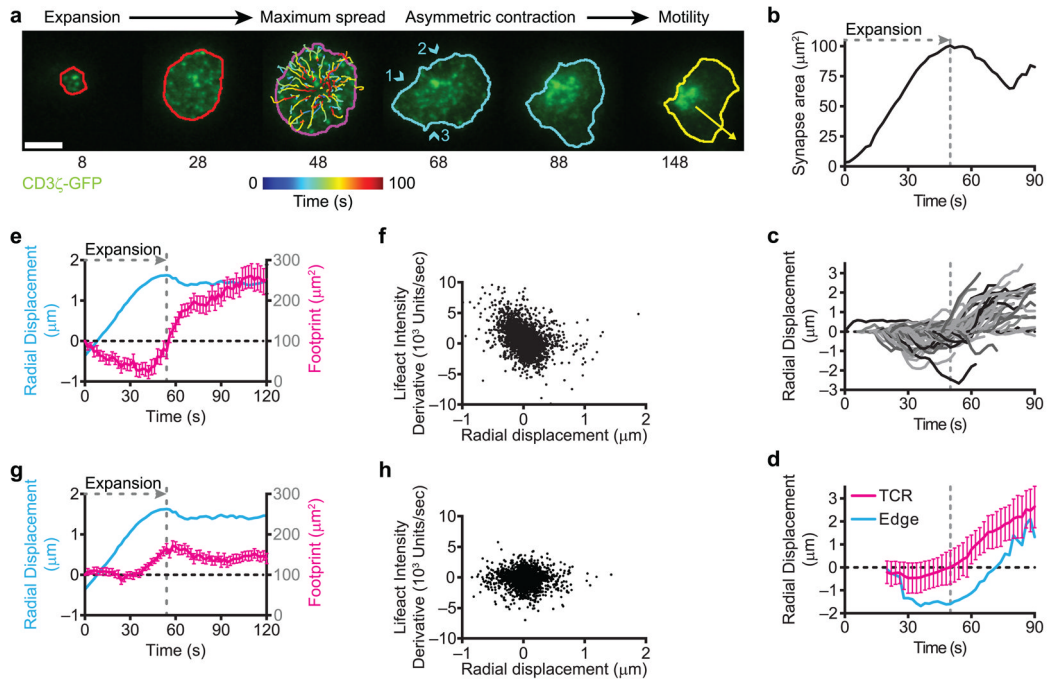
Figure 6. Microcluster centralization correlates with F-actin depolymerization
(**a**) TIRF images of a CD3ζ-GFP[+] OT1^{+} T cell synapse. Numbers below images indicate the time (s) relative to cell-bilayer contact. Scale bar is 5 μm. Light-blue arrow heads indicate the position of edge collapses. Yellow arrow indicates the direction of subsequent motility. Microclusters paths, color-coded by time according to the color bar, are overlaid with the image of the maximally spread synapse. (**b**) Plot of synapse area over time. (**c**) Radial displacement time series of the 111 microcluster tracks. (**d**) The average radial displacement for the 86 microcluster tracks that spanned the expansion-contraction process (magenta) and for the synapse edge (light-blue) at points associated with the microclusters. Error bars are the s.d. For clarity, edge error bars are omitted. (**e,g**) The average radial displacement of microclusters that formed within 2 μm of the synapse edge (**e**) and that formed in the interior (**g**) during synapse spreading by a Lifeact-GFP[+] T cell. The dashed vertical lines in (**b–d,e,g**) correspond to the maximum synapse areas. (**f, h**) Correlation between Lifeact-GFP intensity changes in the 1 μm^2 regions centered on the microclusters and the microcluster radial movements. Movements toward the synapse center are positive, while outward movement is negative. Edge microclusters are shown in (**f**), interior microclusters in (**h**). Results in (**e–h**) are representative of 8 synapses in which Lifeact-GFP was imaged during spreading and contraction.
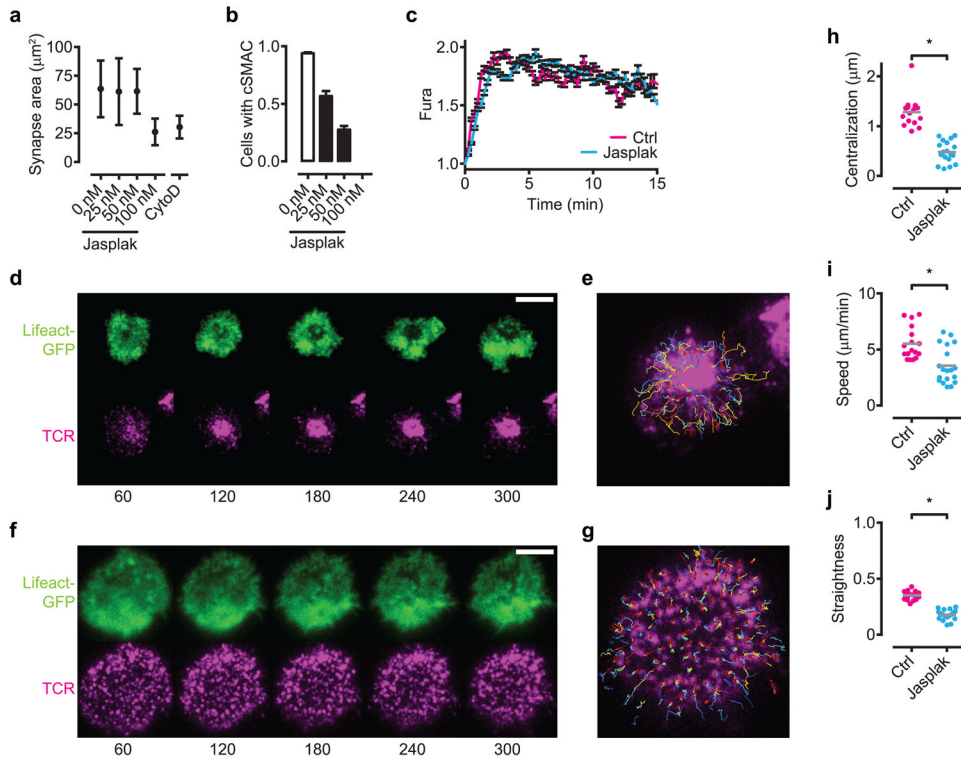
Figure 7. TCR centralization requires actin depolymerization

(**a**) Synapse areas formed by OT1^{+} T cell blasts after treatment with DMSO vehicle, the indicated concentration of jasplakinolide or 10 μM cytochalasin D. (**b**) The fractions of OT1^{+} T cell blasts forming cSMACs after treatment with DMSO vehicle or the indicated concentration of jasplakinolide. For (**a,b**), N = 90–120 cells total, from four independent bilayers. Error bars represent the s.d. (**a**) or s.e.m. (**b**). (**c**) Calcium fluxes generated by Fura-2 loaded OT1^{+} T cell blasts on stimulating bilayers after treatment with DMSO vehicle or 50 nM jasplakinolide. Error bars represent the s.e.m. for 30 control or drug treated cells. (**d,f**) TIRF images of Lifeact-GFP (top) and TCRs (bottom) during synapse formation by a control OT1^{+} T cell blast (**d**) and an OT1^{+} T cell blast treated with 50 nM jasplakinolide treated (**f**). Numbers in (**d,f**) indicate the time (s) relative to the start of spreading. Scale bars are 5 μm. (**e,g**) Microcluster paths overlaid onto images of the cells from (**d,f**), respectively. (**h–j**) Median microcluster centralizations (**h**), average microcluster track speeds (**i**) and mean track straightness (**j**) during synapse formation by control cells and cells treated with 50 nM jasplakinolide. Data represent 16 control and 18 jasplakinolide treated cells. Gray bars represent the mean of the groups (p < 0.009 for all comparisons; Student's t test).